JGR: Planets

Supporting Information for

3D architecture of Kodiak butte as evidence of fluvial or shoal-water environments in Jezero crater, Mars

O. A. Kanine[1], M. P. Lamb[1], B. L. Ehlmann[1], J. P. Grotzinger[1], C. D. Tate[2]

[1]Division of Geological and Planetary Sciences, California Institute of Technology, Pasadena, CA, [2]Department of Astronomy, Cornell University

Contents of this file

Additional Supporting Information (Files uploaded separately)

Introduction

Within this document there are additional details on the process of plane-fitting (Text S1), including the location of beds analyzed (Figures S1-S5). The best fit solutions of each bed orientation are in Data Set S1 (ds01.xlsx). Then follows a description of the process of grain counting (Text S2), details on the image resolutions (Table S1), locations of counts (Figures S6-S8) and detailed results of the grain counts (Figure S9, Table S2) used to determine the median grain size used in paleohydraulic calculations. Raw grain size measurements are in Data Set S2 (file ds02.xlsx). Bar front heights are in Figure S10 and Tables S3 and S4, and the discharge estimates are presented in Figure S11 and Table S5. Terrestrial analogs for large-scale braid bar deposits, mouth bar deposits, and Gilbert deltas are given in Tables S6-S8, respectively.

S1 Bed orientations

288 traces were taken across the Kodiak model along segments of beds that can be locally approximated as planar. These were placed into 21 groups (named Group A through U) which sample Units 2, 3, and 4 (Figure S1). Detail views of trace locations and the plane fits for each group are presented in Figures S2-S4, while Figure S5 shows the orientations of beds organized by both group and unit. Individual plane fits corresponding to the labeled traces in Figures S2-S4 may be found tabulated in the file *ds01.xlsx*.

Data Set S1. A spreadsheet of best-fit solutions for bed orientations is found as *ds01.xlsx*. Beds are organized by "Group" (see Figures S1-S5), and the dip angle, dip azimuth, strike, minimum angular error (Min_e), maximum angular error (Max_e), and rake of each fitted plane is given.

Data Set S2. File *ds02.xlsx* is a spreadsheet of grain lengths, ordered largest to smallest, and the calculated fraction finer using Equation S1.

S2 Grain counts

Grain size counts on the eastern face of Kodiak were performed in two boxes, measuring ~19 m x ~7 m (box 1) and ~8.2 m x ~10 m (box 2) (Figure S6) that sample representative Unit 3 strata along the beds used for paleochannel depth estimates (Figure S5a). To facilitate interval-based sampling analogous to a Wolman pebble count performed in the field (Wolman, 1954), Box 1 contains a grid with 7,367 intersections overlaid on SuperCam image scam01063 and Box 2 contains 4,588 intersections overlaid on SuperCam image scam01077. Both images were color stretched to the minimum and maximum values of the current view extent while counting and were manually co-registered to corresponding sol Mastcam-Z images using a linear fit to facilitate direct comparison between the instrument datasets. Various criteria were used to identify grains, including: color; shape (rounded); relief (as indicated by shadowing) from the surrounding rock; visibility in different images (i.e., observable in both the aforementioned sol 63 and sol 77 SuperCam images) where available to represent different lighting conditions, view angles, and image stretches; not talus; not cut by visible layers aligned with the surrounding bedding fabric; and not associated with other confounding features such as a fracture or a weathering-resistant bed with knobby texture. We recognize that these criteria bias the count toward larger, darker grains that contrast against the surrounding rock, and may have eliminated some real grains from the count. Nevertheless, in absence of physical access to the outcrop, we favor greater certainty over over-interpretation of long-distance images in service of producing order-of-magnitude estimates of the hydrology of the depositing flow, and favor consistent, rule-based counts in service of scientific reproducibility. While not counted, one may note a "mottled" texture in the SuperCam images, especially in rubbly-textured beds, which may indicate the presence of clasts with diameters around or just below the imaging resolution (Morgan et al., 2014) (i.e., ~2.5 cm for the sol 63 SuperCam image (Table S1)); this is consistent with our estimates of a D_{50} between ~1 and ~3.6 cm. We also note this range is aligned with the proposed grain size of Catuneanu et al. (2023). We choose the value of 2.6 cm for hydrology calculations as it is derived from the most heavily sampled bin and close to the mean calculated D_{50} of 2.3 cm for all bins.

The longest axis exposed on the identified grains was recorded (Figures S7, S8). Physical lengths were calculated by multiplying the length of the traced axis in pixels by the image resolution (Table S1). The summary of the count is presented in Figure S9. Grains were counted if their boundaries appeared to be within 1 pixel width of the grid intersection, and if a grain crossed more than one intersection on the grid, each overlapped intersection was counted. We infer that the visible grains comprise the coarsest fraction of the sedimentary deposit, and that every intersection where a grain was not visible, the grain present must be too small to be resolved (i.e., < 7.4 cm for the sol 63 SuperCam image). Following this logic, we can estimate the percentage of the outcrop finer than a given grain, starting with 100% of the grains in the box being smaller than the largest counted grain. The D_{50} may then be estimated from this coarse fraction using the cumulative distribution function in Equation S1, which assumes a log-normal distribution for the sediment sizes (Parker, 2004). We assume that $D_{84}/D_{50} = 2$. The results of the D_{50} calculation are presented in Table S2.

$$f_{finer} = \frac{1}{2}\left[1 + erf\left(\frac{lnD_{bin} - lnD_{50}}{\sqrt{2}ln\frac{D_{84}}{D_{50}}}\right)\right] \qquad \textbf{Equation S1}$$

S3 Paleo-discharge

We utilize our estimates of channel geometry, bedload grain size, and empirical relationships for terrestrial rivers to constrain the magnitude of the flow that deposited Kodiak. First, we may use the relationship between bankfull stress (τ_*) for steady uniform flow (Equation S2) and the critical Shield's number (τ_{*c}) for incipient particle motion in coarse, braided rivers (Equation S3, Paola and Mohrig, 1996) to solve for channel slope (S) (Equation S4, Lamb et al., 2008). R, the submerged specific gravity of sediment, is assumed to be 2.0 for a basaltic bedload. For a sand-bedded river, we infer most of the flow resistance is due to large-scale bedforms (e.g. Paola and Mohrig, 1996; Parker and Peterson, 1980) and thus the equations below remain valid.

$$\tau_* = \frac{dS}{RD_{50}} \qquad \textbf{Equation S2}$$

$$\tau_* \approx 1.4\tau_{*c} \qquad \textbf{Equation S3}$$

$$\tau_{*c} \approx 0.15\left(S^{0.25}\right) \qquad \textbf{Equation S4}$$

Combining equations S2 - S4 gives:

$$S = \left[\frac{100}{21}\left(\frac{d}{RD_{50}}\right)\right]^{-\frac{4}{3}} \qquad \textbf{Equation S5}$$

We use the variable-power resistant formula for gravel and boulder-bedded rivers (Equation S6) proposed in Ferguson, 2007 with parameters $a_1 = 6.5$ and $a_2 = 2.5$ (Ferguson, 2007) to calculate a friction factor f, assuming $D_{84} \approx 2D_{50}$ ($D_{84} = 2.2D_{50}$ used in Rickenmann

and Recking, 2011, and $D_{84}= 2D_{50}$ used in Morgan et al., 2014) and thus calculate bankfull flow velocity using the Darcy-Weisbach formula (Equation S7, Silberman et al., 1968). We set the gravitational constant g = 3.72 m/s^2 for Mars. Flow depth *d* is estimated from measurements of bar strata heights in Unit 3 (Figure S10; Table S3, S4).

$$\sqrt{\frac{8}{f}} = 16.3\left(\frac{d}{D_{84}}\right)\left[42.3 + 6.3\left(\frac{d}{D_{84}}\right)^{\frac{5}{3}}\right]^{-\frac{1}{2}} \qquad \textbf{Equation S6}$$

$$u = \sqrt{\frac{8gdS}{f}} \qquad \textbf{Equation S7}$$

We may now calculate discharges for a range of channel geometries, with $Q = udw$. Studies of terrestrial gravel bed rivers indicate braiding initiates at a width-to-depth (w:d) ratio of approximately 50 (Eaton et al., 2010; Kleinhans et al., 2011). The upper bound of w:d values is less well-constrained. The dataset of braided rivers in Li et al. (2023) have w:d between ~20 and ~400, while the compilation of sand to cobble/boulder bedded braided and braided/anastomosing rivers in Church and Rood's 1983 dataset have w:d from 35 to 371. Thirteen braided or moderately braided rivers with recorded bankfull widths and depths in Kleinhans and van den Berg (2011) show a range of width-to-depth values of ~60 to ~2090. While there are braided and low-sinuosity rivers with w:d > 1000 (Parker, 1976; Gibling, 2006), most fall within 50 < w:d < 1000 (Gibling, 2006). We utilize width-to-depth ratios 50 - 400 to represent a broad range of plausible bankfull channel geometries for this system.

Using D_{50} = 2.6 cm, *d* = 4.2 (Table S4), and R = 2.0 for specific gravity of basaltic sediment bedload, we find a slope of 0.00036, a friction factor f = 0.044, and velocity u = 1.01 m/s. For a sand-bedded river with D_{50} = 2 mm, we find a slope S = 9.5 x 10^{-6}, f = 0.0187, and u = 0.25 m/s. We present our estimates of river discharge in Table 5 and Figure S11.

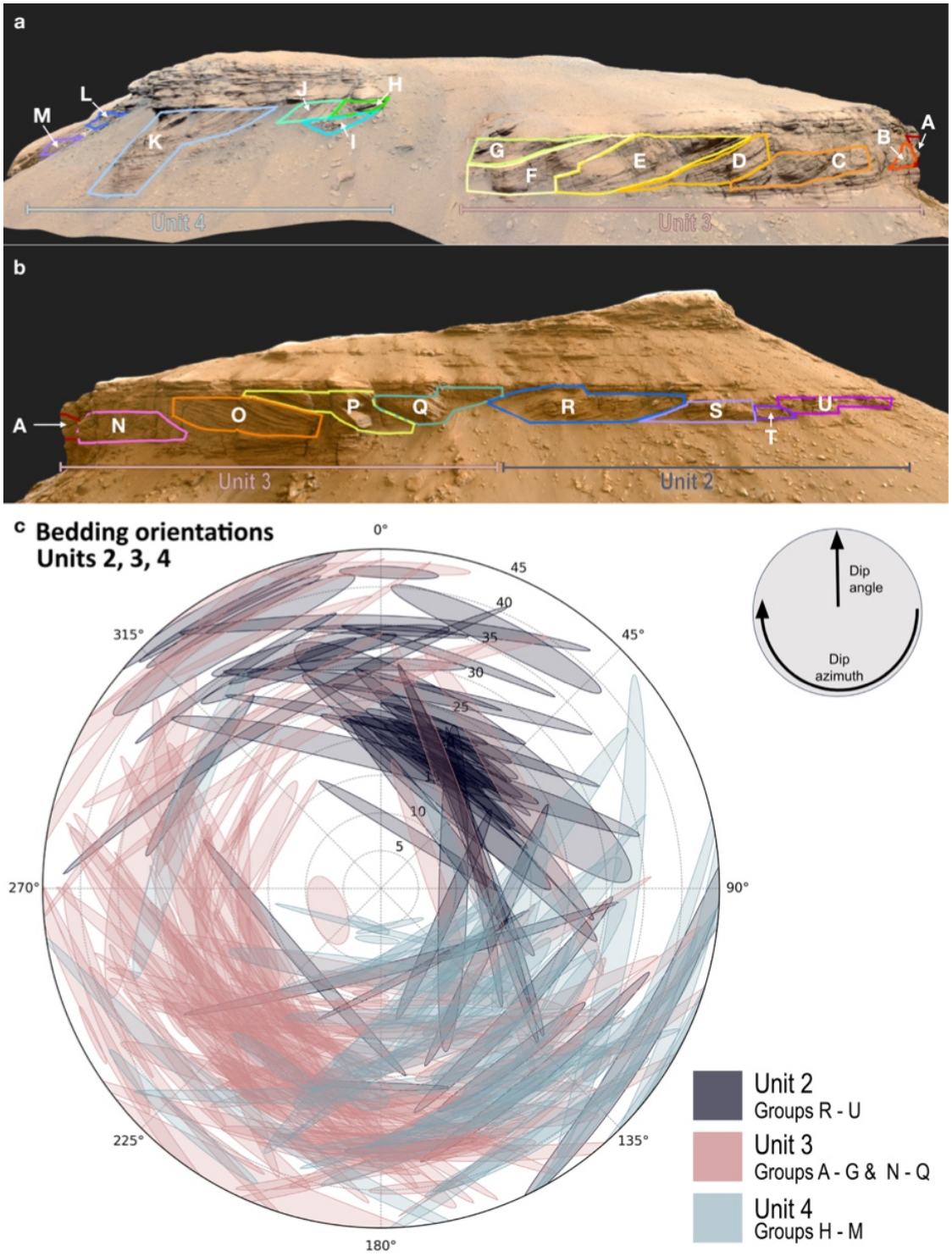

Figure S1. Bedding orientations. Part **a** shows the east face of Kodiak and sample groups A - M, which comprise units 1 and 2. Part **b** shows sample groups A and N - U on the north face of Kodiak, which make up sequences 2 and 3. Plane fits for traces in units 2, 3, and 4 are plotted in part **c** to the 95th percent confidence interval using methodology of Quinn and Ehlmann (2019). Dip azimuth is read on the perimeter of the plot, with north as 0˚, and dip angle increases radially outward from the center of the plot (see key in upper right of part **c**).

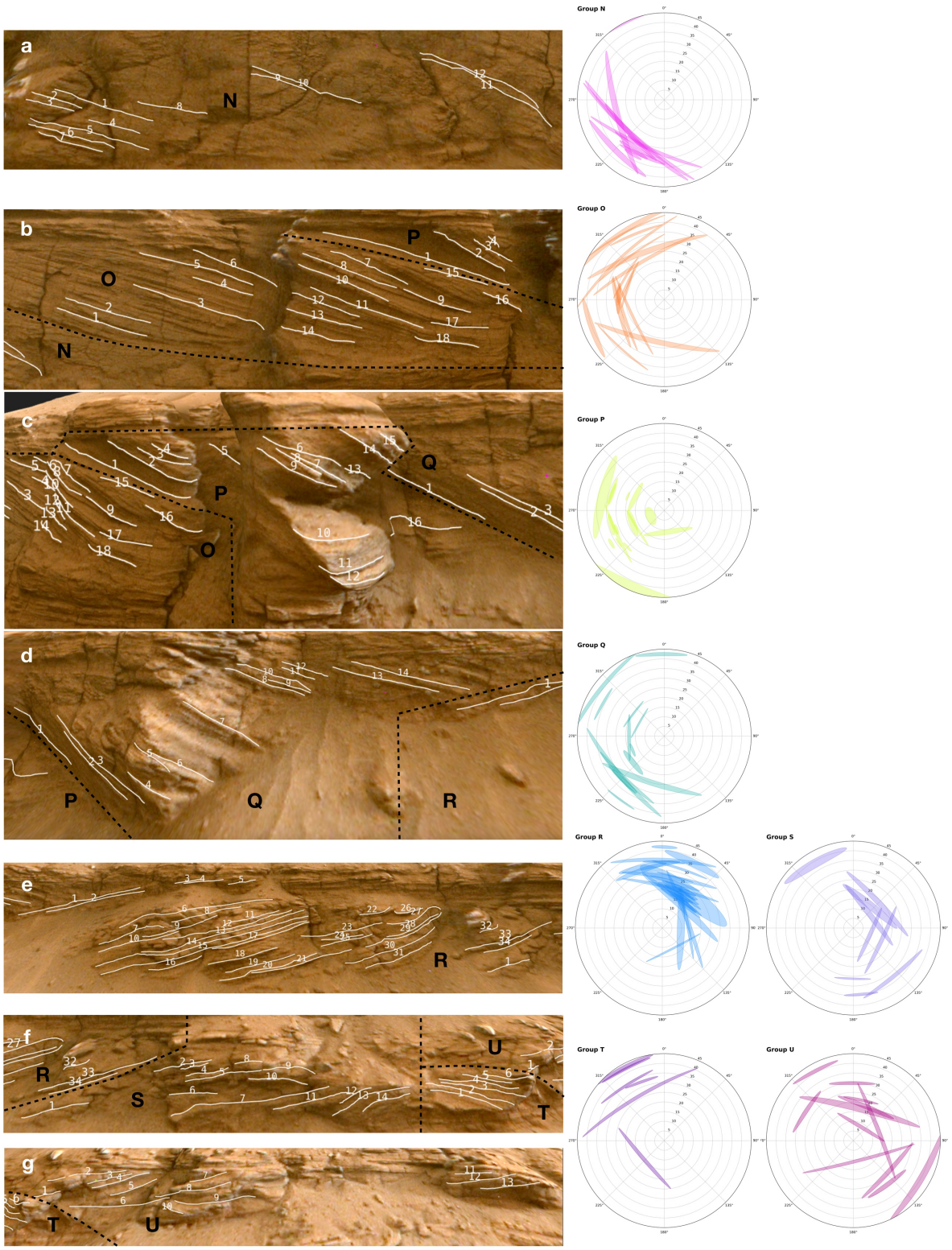

Figure S2. Trace locations (parts **a-g**) and plane fits (right) for sampling groups N-U, associated with Units 2 and 3. Colors of bed orientation plots correspond to group outlines in Figure S1.

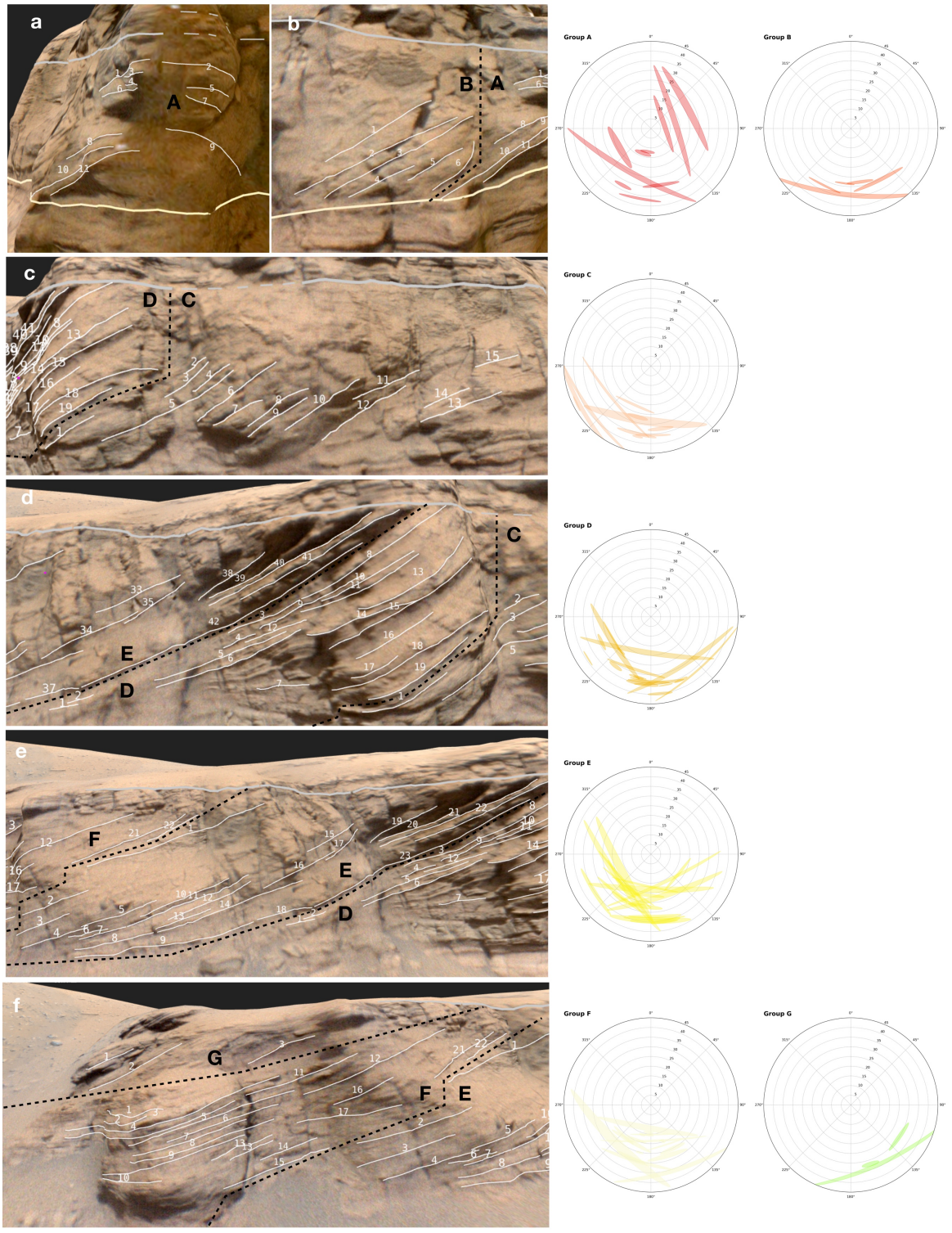

Figure S3. Trace locations (parts **a-f**) and plane fits (right) for sampling groups A-G, associated with Unit 3. Colors of bed orientation plots correspond to group outlines in Figure S1.

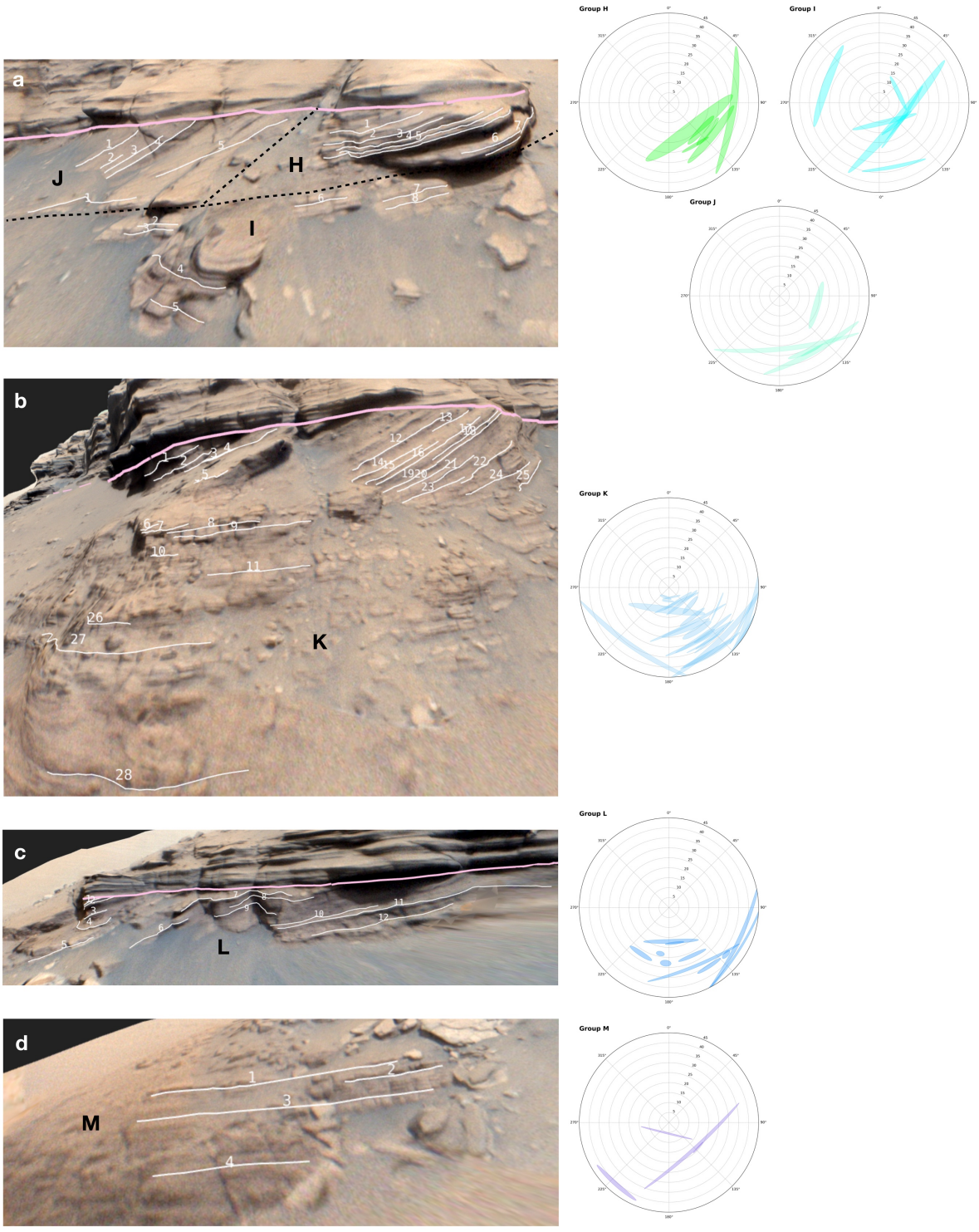

Figure S4. Trace locations (parts **a-d**) and plane fits (right) for sampling groups J-M, associated with Unit 4. Colors of bed orientation plots correspond to group outlines in Figure S1.

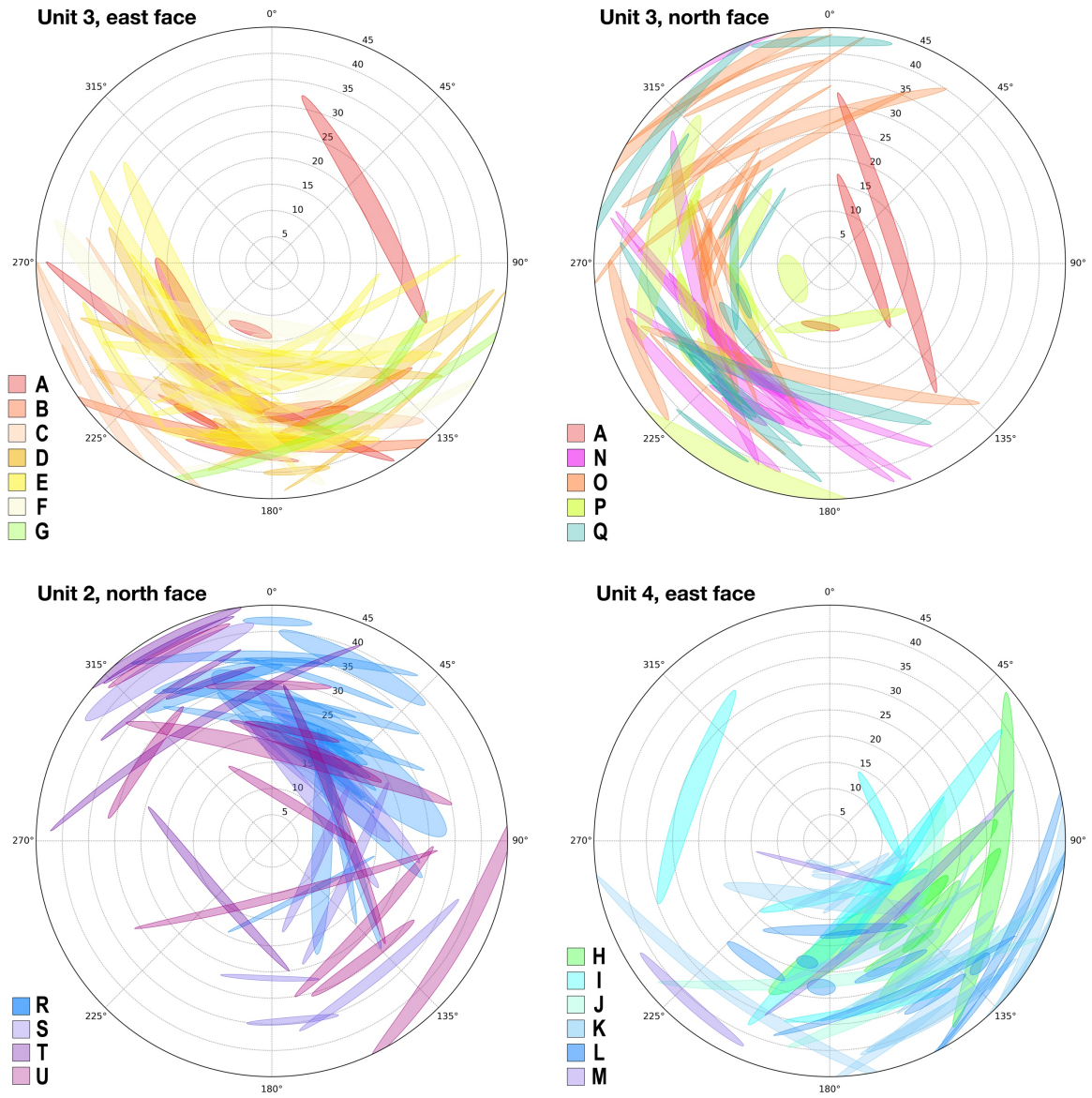

Figure S5. Bed orientations of each group organized by unit. Unit 3 is divided into the exposures on the east and north face of Kodiak.

Instrument	Sol	Sequence ID	Distance (rover to target, m)	Resolution (cm/px)	Smallest resolvable feature (3 pixels wide, cm)
Mastcam-Z	63	zcam08022	2369	17	51
	77	zcam08036*	2390	17	51
	409	zcam08425	784	5.5	17
	415	zcam08430	527	3.7	11
	416	zcam08433	478	3.3	9.9
SuperCam	63	scam01063	2369	2.47	7.4
	77	scam01077	2390	2.50	7.5
	418	scam01418*	478	0.50	1.5
	548	scam04548*	580	0.61	1.83
	580	scam01580	701	0.73	2.19

Table S1: Key images of Kodiak with their resolutions and the size limits of resolvable grains. *Images are usable for some visual analysis but were not incorporated into the 3D model.

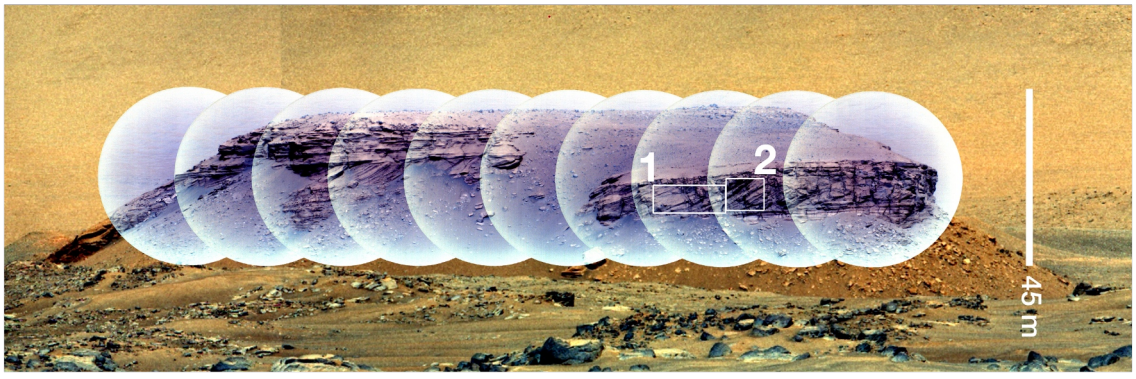

Figure S6. Grain count sample locations over sol 63 Mastcam-Z (zcam08022) and SuperCam (scam01063) color-enhanced mosaics.

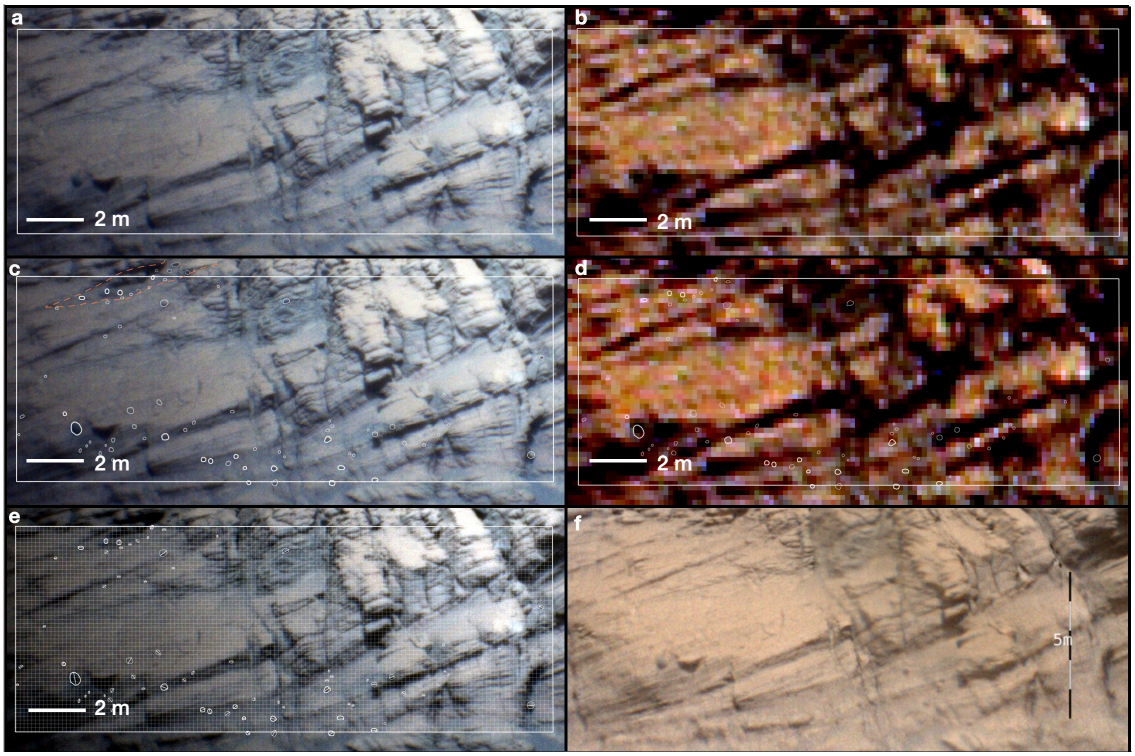

Figure S7. Grain counts and comparison of SuperCam and Mastcam-Z images, box 1. Parts **a**, **c**, and **e** utilize a sol 63 SuperCam frame, while **b** and **d** use a sol 63 Mastcam-Z image. The white box in all parts of this figure shows the extent of the grid used for grain counting in Box 1. Parts **c** and **d** include outlines of identified grains, and **c** shows a coarse lens in dashed red line; **e** shows the grid partially transparent over the base SuperCam image in addition to the grain outlines and long axis measurement locations. Part **f** shows approximately the region sampled in **a**-**e** as viewed on the 3D model looking to the east.

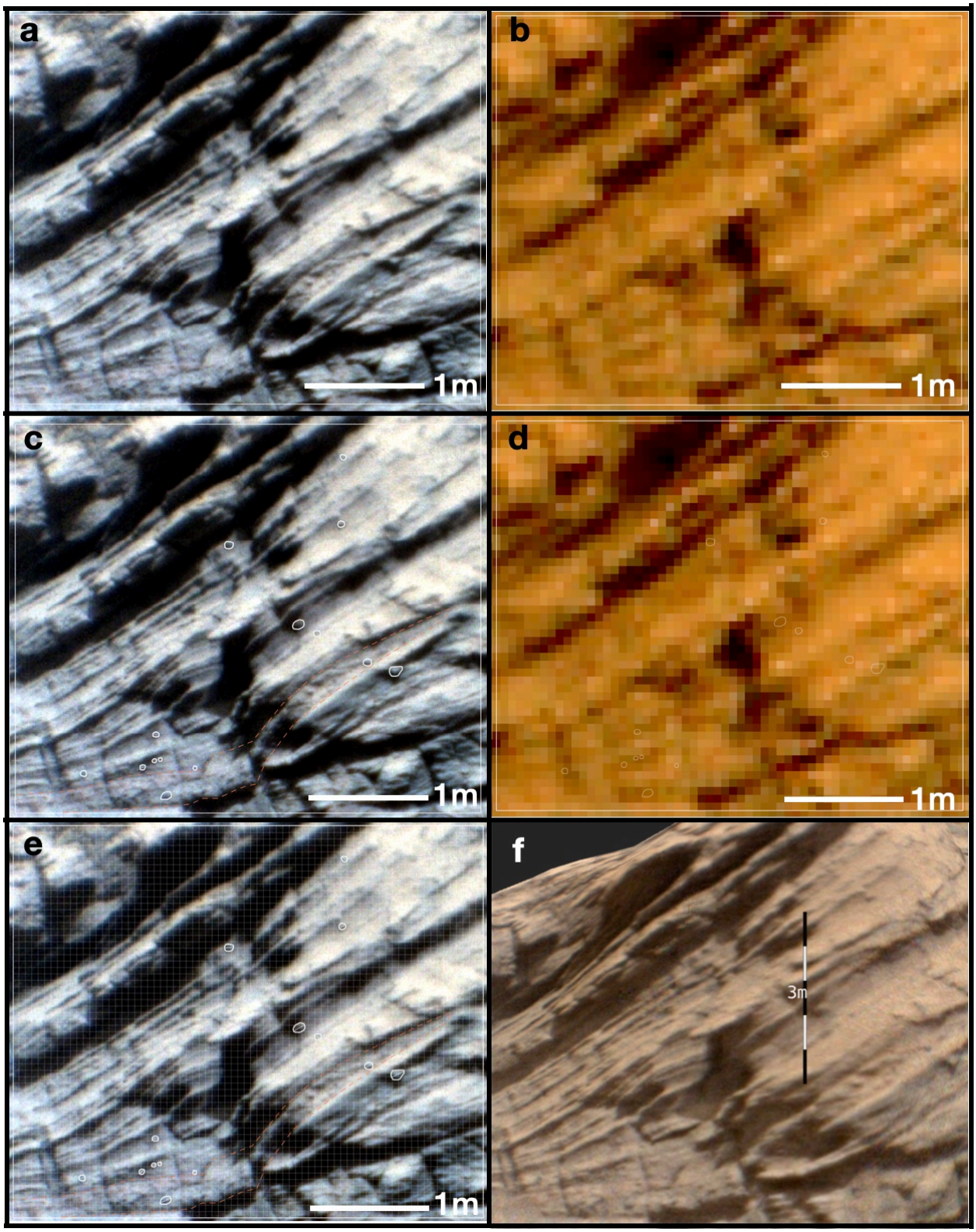

Figure S8. Grain counts and comparison of SuperCam and Mastcam-Z images, box 2. Parts **a**, **c**, and **e** utilize a sol 77 SuperCam frame; **b** and **d** use a sol 77 Mastcam-Z image. The white box in all parts of this figure shows the extent of the box 2 grid used for grain counting. **c** and **d** include outlines of identified grains and a coarse lens (red dashed line); **e** shows the grid partially transparent over the base SuperCam image in addition to the grain outlines and long axis measurement locations. Part **f** shows approximately the region sampled in **a**-**e** as viewed on the 3D model looking to the east.

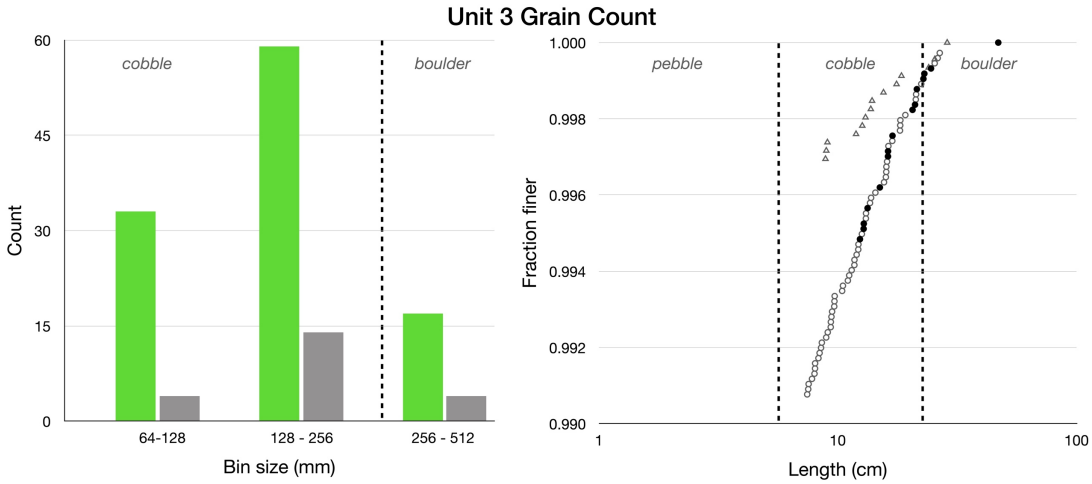

Figure S9. Histogram and fraction finer calculations for Unit 3. The green bars are counts from Box 1, while grey show results from Box 2; filled black circles are high-confidence grains from Box 1, and open circles show the remaining mapped grains. Triangles show grains mapped from Box 2.

Sample	Image	Bin [mm]	Count	f_{finer}	Calculated D_{50} [cm]
Box 1	scam01063	64 -128	33	0.985	1.4
		128 - 256	59	0.990	2.6
		256 - 512	17	0.998	3.6
Box 2	scam01077	64 -128	4	0.995	1.1
		128 - 256	14	0.996	2.0
		256 - 512	4	0.999	2.9

Table S2. Grain count results from Unit 3. D_{50} is extrapolated from the measured grains in each bin (assumed to be the coarse fraction) using equation S1.

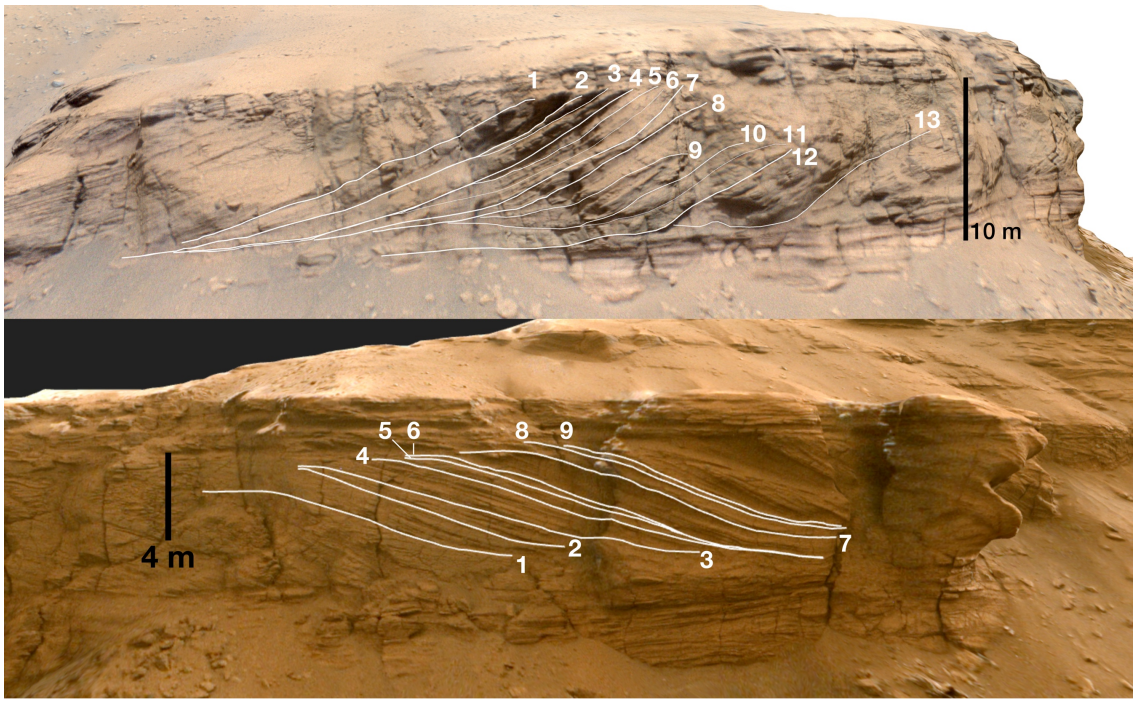

Figure S10. Locations of Unit 3 bed height measurements, east face on top and north face below. Values are reported in Tables S3 and S4.

North face	
Trace	Height [m]
1	3.1
2	3.8
3	4.1
4	4.8
5	4.8
6	4.9
7	4.1
8	4.2
9	3.9

Table S3. Vertical height of inclined beds on north face (Fig. S10, bottom).

East face	
Trace	Height [m]
1	8.9
2	10.1
3	10.6
4	10.1
5	10.2
6	10.0
7	10.1
8	7.9
9	4.1
10	5.2
11	5.1
12	6.4
13	5.6

Table S4. Vertical height of inclined beds on east face (Fig. S10, top).

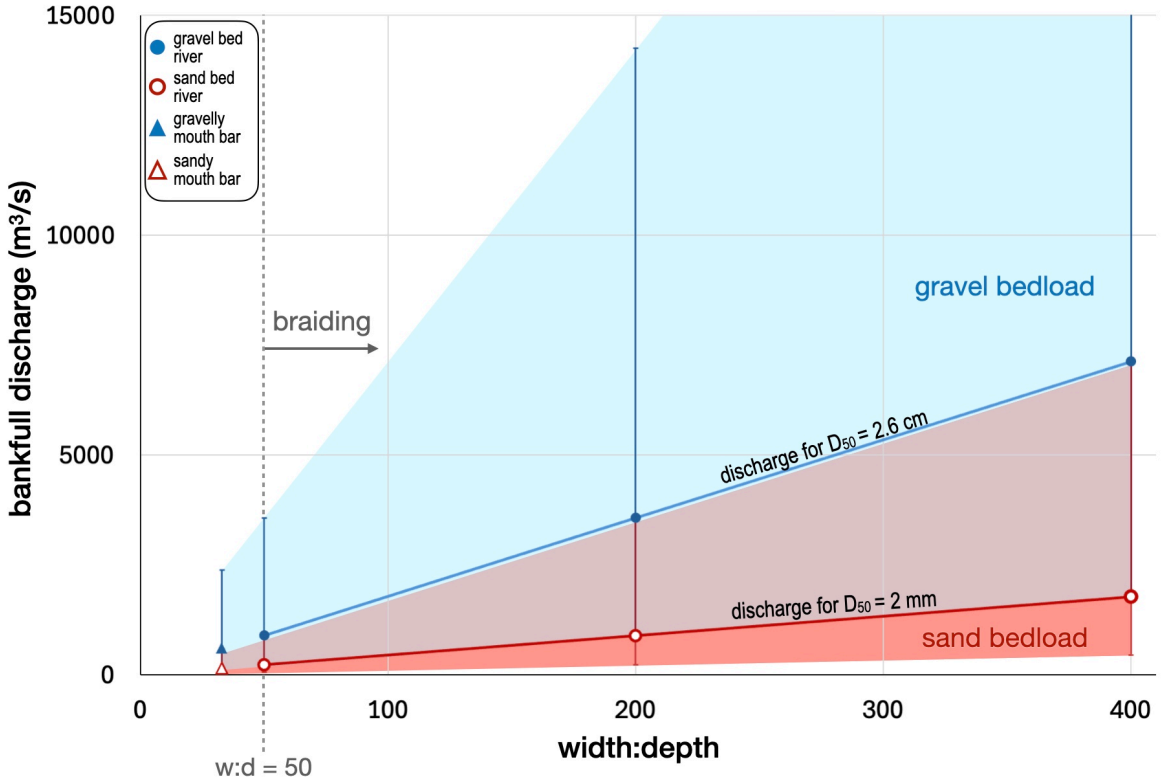

Figure S11. Discharge estimates based on Unit 3 strata height measurements yielding estimated bankfull flow depth of 4.2 m. Blue shaded region uses calculated D_{50} of 2.6 cm, slope = 0.00036, and u = 1.01 m/s. Red shaded region uses D_{50} = 2 mm, slope = 9.5 x 10^{-6}, and u = 0.25 m/s. Purple shaded region shows discharges plausible for either a gravel bed or sand bed of a given width:depth. Circles represent estimates for braided rivers at w:d = 50, 200, and 400; triangles are estimates for mouth bars, using the width of the Unit 3 form as an upper bound for channel width and yielding w:d = 33. Error bars show a factor of 6 error, as both the bankfull flow depth and the flow velocity carry an error of ~ a factor of 2 (Hayden and Lamb, 2020; Mohrig et al., 2000; Ferguson et al., 2007) and depth was used with an assumed w:d to find width.

Environment	Width-to-depth	Discharge [m^3/s]
Gravel-bed braided river	50	890
	200	3,600
	400	7,100
Sand-bed braided river	50	220
	200	880
	400	1800
Gravelly mouth bar	33	590
Sandy mouth bar	33	150

Table S5. Estimated bankfull discharge rates for range of channel geometries and bed types for mouth bars and braided rivers.

Literature examples of terrestrial steep river bar strata	
Source	*Description*
Figures 4 and 6 in Almeida et al., 2016 https://doi.org/10.1111/sed.12230	Unit bar fronts with multiple meters of relief in the Hawkesbury Sandstone in southeast Australia and the Marizal Formation in northeastern Brazil.
Figures 9 and 10 in Steel and Thompson, 1983 https://doi.org/10.1111/j.1365-3091.1983.tb00677.x	Conglomeratic braid bar fronts several meters in height in the Bunter Pebble Beds, England.
Figure 4 in Carling et al., 2013 http://dx.doi.org/10.1016/j.earscirev.2013.06.002	Pebbly sandstone and boulder conglomerate bar front beds with several meters relief deposited via megafloods in the Altai Mountains.
Figures 11 and 14 in Cowan, 1991 https://doi.org/10.2110/csp.91.03.0080	Fill of multi-meter deep scour hole or "hollow" by sandstone avalanche faces at braid channel confluences or upstream of a large bar. Morrison Formation, New Mexico.

Table S6. Compilation of terrestrial field examples of sandy and gravelly steeply-inclined braided river strata.

Literature examples of terrestrial mouth bars in shallow deltas	
Source	*Description*
Figure 9 in Gruszka and Zielinski, 2021 https://doi.org/10.2478/logos-2021-0004	~1 m thick gravelly mouth bar with sigmoidal beds, deposited in a shallow glacial lake, Poland.
Figure 10 in Lesczcyński and Nemec, 2015 https://doi.org/10.1111/sed.12155	Gravelly mouth bar (<1 m thick) with sigmoidal beds deposited in shoal-water or mouth bar-type delta, Poland.
Figure 4a and 7d in Winsemann et al., 2021 https://doi.org/10.1016/j.sedgeo.2021.105962	Gravelly sub-meter to >2 m thick shallow-water mouth bar deposits with tangential beds in Germany and Spain.
Figure 6d in Schomacker et al., 2010 https://doi.org/10.1111/j.1365-3091.2009.01136.x	Sandy mouth bar ~5 m thick deposited in shallow lake. Green River Formation, Utah.

Table S7. Compilation of terrestrial field examples of sandy and gravelly shallow-water mouth bars with inclined beds.

Literature examples of terrestrial Gilbert deltas	
Source	*Description*
Figures 2 and 19 in Bell, 2009 http://dx.doi.org/10.5027/andgeoV36n1-a04	Gilbert delta deposits in Lake General Carrera, Chile. Broad, arcuate fronts shown in planview in Figure 2, and conglomeratic delta foresets shown in cross-section in Figure 19.
Figure 1 in Lai et al., 2019 https://doi.org/10.1029/2018WR023824	Gilbert delta in Peyto Lake, Canada with straight shoreline and braided channels on delta top.
Figure 1 in Ke and Capart, 2015 http://dx.doi.org/10.1002/2015GL066455	Gilbert delta with straight shoreline in Wushe reservoir, Taiwan.

Table S8. Compilation of terrestrial field examples of gravelly, homopycnal Gilbert deltas, exhibiting typical smooth, straight-to-arcuate shorelines in planview.